Materials Research Bulletin 140 (2021) 111310

Contents lists available at ScienceDirect

Materials Research Bulletin

journal homepage: www.elsevier.com/locate/matresbu

Egg white derived carbon materials as an efficient sulfur host for high-performance lithium-sulfur batteries and its electrochemical properties

B.S. Reddy [a], M. Premasudha [a], Kwang-Moon oh [a], N.S. Reddy [b], Jou-Hyeon Ahn [a,c,*], Kwon-Koo Cho [a,*]

[a] Department of Materials Engineering and Convergence Technology & Research Institute for Green Energy Convergence Technology, Gyeongsang National University, 501 Jinju-daero, Jinju 52828, Republic of Korea
[b] School of Materials Science and Engineering, Engineering Research Institute, Gyeongsang National University, 501 Jinju-daero, Jinju 52828, Republic of Korea
[c] Department of Chemical Engineering and Research Institute for Green Energy Convergence Technology, Gyeongsang National University, 501 Jinju-daero, Jinju 52828, Republic of Korea

ARTICLE INFO

Keywords:
Cheese-like carbon
Egg white
Sulfur
Lithium-sulfur batteries

ABSTRACT

Lithium-sulfur (Li-S) batteries are attractive and prominent power sources due to high theoretical capacity and the availability of sulfur at a low price. However, sulfur has limitations such as the formation of polysulfides and low conductivity. To overcome these problems, we prepared a cheese-like carbon (CLC) using a simple annealing process from an egg white. The as-prepared carbon material contains NaCl and KCl compounds. The CLC with nanoholes were formed after cleaning with distilled water and ethanol several times. The prepared CLC had a strong polysulfide capturing ability, high conductivity, a large surface area, and high catalytic activity. To prepare the CLC/S composite, sulfur was added by the melt diffusion method. CLC/S cathode material exhibited a high initial capacity of nearly 1420 mA h g^{-1} at 0.1 C and excellent rate capability with a low capacity-fading rate. The present work revealed that CLC/S cathodes are potential candidate cathodes for Li-S batteries.

1. Introduction

Advanced lithium-ion battery (LiBs) technology has a vital role in transportable electronics and mobile electronic devices [1–3]. However, LiBs cannot be used in large-scale applications due to their lower theoretical capacity and energy density [4,5]. Recently, Li-S batteries have attracted interest as a replacement for LiBs batteries in large scale applications and portable electronic devices due to their higher theoretical capacity (1672 mA h/g) and energy density [6,7]. Also, sulfur is abundant, eco-friendly, non-toxic, and has a low cost which makes it ideal for large-scale applications [8,9]. However, Li-S has some limitations such as low conductivity, high volume expansion, and the formation of lithium polysulfides. This leads to low sulfur utilization and fast fading capacity results in poor coulombic efficiency [10].

Therefore, researchers are focused on developing high-performance Li-S batteries. To solve these difficulties through the utilization of cathode composites, an effective strategy has been designed to load the high sulfur content by natural carbon resources, such as through soybeans [11], shrimp shells [12], pomegranates [13], oak fruit trees [14], bamboo [15] and litchi shells [16] to synthesize the porous carbon structure as a conductive matrix for Li-S batteries. Moreover, Bingan Lu et al. synthesized low cost materials into a carbon foam with a microporous structure wherein biomimetic carbon cells showed excellent electrochemical properties of potassium ion batteries [17,18]. Apparao M.Rao and Bingan Lu et al. prepared the layered graphene microspheres and the prepared anode material exhibited excellent electrochemical properties when compared with other graphene based electrodes [19]. The porous carbon was synthesized by the hydrothermal method, template synthesis method, activation, and carbonization method. Among these, the carbonization method is easiest to prepare for carbon material. The carbon material derived from egg whites has a complex CLC structure which results in a well-developed, nanohole architecture with high pore volume, specific surface area, and available self-nitrogen content. These are suitable for the impregnation of high loading of

* Corresponding authors at: Department of Materials Engineering and Convergence Technology & Research Institute for Green Energy Convergence Technology, Gyeongsang National University, 501 Jinju-daero, Jinju 52828, Republic of Korea.
E-mail addresses: jhahn@gnu.ac.kr (J.-H. Ahn), kkcho66@gnu.ac.kr (K.-K. Cho).

https://doi.org/10.1016/j.materresbull.2021.111310
Received 24 November 2020; Received in revised form 4 March 2021; Accepted 9 March 2021
Available online 11 March 2021

sulfur, and providing intimate contact between the sulfur and carbon matrix [20–22].

In the present work, we report on the preparation of cheese-like carbon (CLC) with nanoholes acting as hosts to high loads of sulfur, showing its significantly enhanced electrochemical properties as a cathode material for Li-S batteries. As illustrated in Scheme 1, the CLC was synthesized through a simple annealing process using egg whites. The annealed sample was cleaned with distilled water to remove undesired particles like KCl and NaCl. To get the CLC with nanoholes, the obtained product was dried in a vacuum oven. The prepared CLC with nanoholes has a high surface area which contributes to the high loading of sulfur. Besides, the CLC helps to hold the polysulfides and increases the usage of sulfur during cycling. Thus, the prepared CLC/S composite electrodes show good electrochemical performance with a high initial capacity of 1420 mA h/g and good rate performance. This result demonstrates a simple annealing procedure and a low-cost effective approach to superior Li-S batteries.

2. Experimental

2.1. Preparation of cheese-like carbon (CLC) with nanoholes

The chicken eggs were purchased from an open market (Jinju, South Korea). Firstly, the eggs were boiled at 100 °C for 30 min. The egg white was taken from the boiled eggs and annealed at 600 °C under Ar/H_2 atmosphere. The second step was to remove the unwanted particles and adsorbed contaminants in the annealed carbon material by using ultrasonication. The black product was centrifuged (14,000 rpm at 10 min) with distilled water. Finally, the obtained black product was dried in a vacuum oven to get the CLC with nanoholes.

2.2. Preparation of CLC/S composite

The CLC/S composite was prepared by the conventional melt diffusion method. In a typical synthesis, elemental sulfur powder and as-prepared CLC were ground consistently by ball milling. The ground material was moved to an alumina boat and heated at 155 °C for 12 h in an argon atmosphere followed by natural cooling to room temperature. For comparison, uncleaned carbon-sulfur composite (UC/S) is also synthesized through the same procedure.

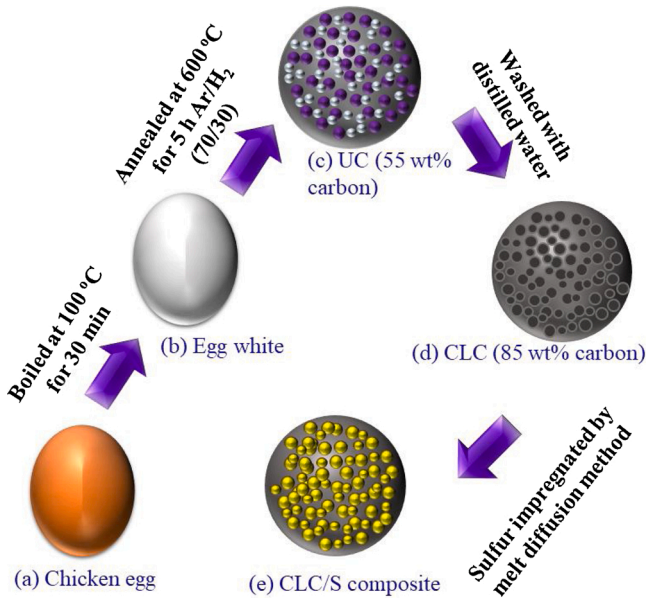

Scheme 1. Fabrication procedure of the CLC and CLC/S composite.

2.3. Physical characterizations

The as-prepared materials crystalline phases were examined by X-ray diffraction (XRD, Bruker co. DE/D2 PHASER). The surface morphologies and selected area elemental mappings were revealed by FESEM (FEI. TF30ST) equipped with an X-ray energy dispersive spectroscopy. The microstructures were analyzed by field-emission transmission electron microscopy FE-TEM (FEI. TF30ST). The N_2 adsorption/desorption isotherms were measured at 77 K with the QUADRASORB SI-MP (Quantachrome). The specific surface area and pore size distribution of the materials were calculated according to the Brunauer-Emmett-Teller (BET) method and Barrett-Joyner-Halenda (BJH) method. Fourier transform Raman spectroscopy was used in an FT-Raman, Bruker FRS-100/S with an Nd: YAG laser at a 1064 nm exciting radiation. The content of the sulfur was analyzed by thermogravimetry analyses (TGA, TA Instruments, and Q50). TGA analysis was conducted from 25 °C to 500 °C at a heating rate of 10 °C min^{-1} in N_2.

2.4. Cell assembly and electrochemical measurements

The electrochemical measurements were conducted on the as-synthesized cleaned cheese-like carbon-sulfur cathode (CLC/S) and an uncleaned carbon-sulfur cathode (UC/S) using a coin cell (coin type 2032) with lithium foil (purity 99.95 %) as the negative electrodes and polypropylene (celgard 2400) as a separator. The electrode was prepared with 80 wt% active materials, 10 wt% acetylene carbon black, and 10 wt% polyvinylidene fluoride (PVDF) dissolved in N-methyl-2-pyrrolidine (NMP) to form a highly uniform slurry. The slurry was coated onto aluminum foil and dried in a vacuum oven at 60 °C overnight. The electrolyte consisting of 1 M LITFSI was dissolved in a mixed solvent of 1,3DOL and 1, 2DME (1:1, v/v) electrolyte. The loading of sulfur is about 1.0–1.2 mg/cm^2 in the electrode, and the prepared electrolyte used 30 μL for each coin cell. Cell assembly was performed in an argon gas-filled glove box. The galvanostatic cycling was performed using a WBCS3000 battery cycler (Won-A Tech. Co.) at room temperature with the voltage range of 1.7–2.8 V. The electrochemical impedance spectroscopy (EIS) measurements were conducted within a frequency range of 0.1−100 MHz.

3. Results and discussion

The experimental procedure of the CLC and CLC/S from the egg white is shown in Scheme 1. Fig. 1(a) shows the XRD patterns of CLC and uncleaned carbon (UC) materials. The egg-white contains Na and K elements. Sodium and potassium are indispensable elements in the biological systems, and therefore, after annealing at a high temperature, these two elements were crystallized out in the form of NaCl and KCl. After cleaning with distilled water, NaCl and KCl dissolved in distilled water and were removed through centrifugation. The XRD results demonstrate that no NaCl and KCl remained in the carbon. It is believed that the holes will form throughout the whole carbon, not just only on the surface. Fig.1 (b) shows the Raman spectroscopy for an additional check of the carbon present in the CLC, UC, and CLC/S materials. The two main peaks around 1357 and 1595 cm^{-1} consists of D and G-bands of as-prepared materials. The intensity ratio of the $I_{D/G}$ for CLC and UC is 1.28 and 1.25, respectively. The CLC has a higher-intensity ratio than UC, indicating the CLC has a more defective nature attributed to the highly porous structure. For the CLC/S composite, the intense Raman peaks show at 151, 216, and 410 cm^{-1}, corresponding to the elemental sulfur. The elemental sulfur peaks and the broadening of the D band display that sulfur successfully doped into the carbon nanoholes.

Fig. 2 illustrates the SEM images, EDS investigation, surface area, and pore size distribution of the CLC. Fig. 2 (a) shows the SEM and EDS analysis of the decomposition product of boiled egg white after centrifugation washing with distilled water and ethanol. According to the SEM image, the NaCl and KCl crystallized out after washing, and those places

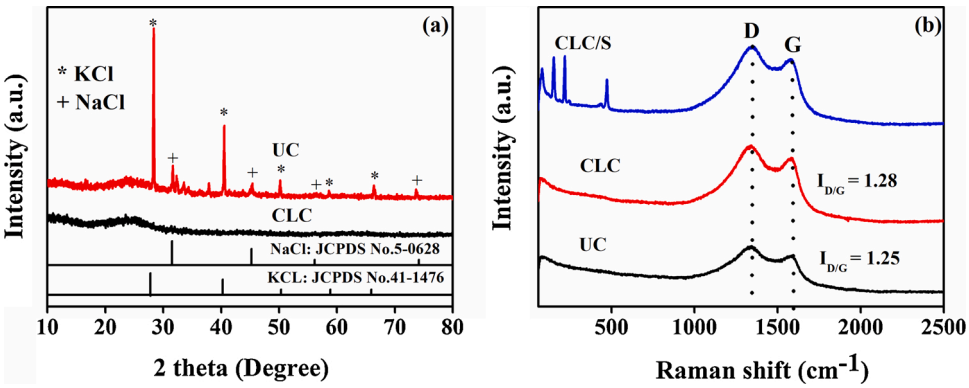

Fig. 1. (a) XRD patterns of CLC and UC, and (b) Raman spectra of the UC, CLC, and CLC/S composite.

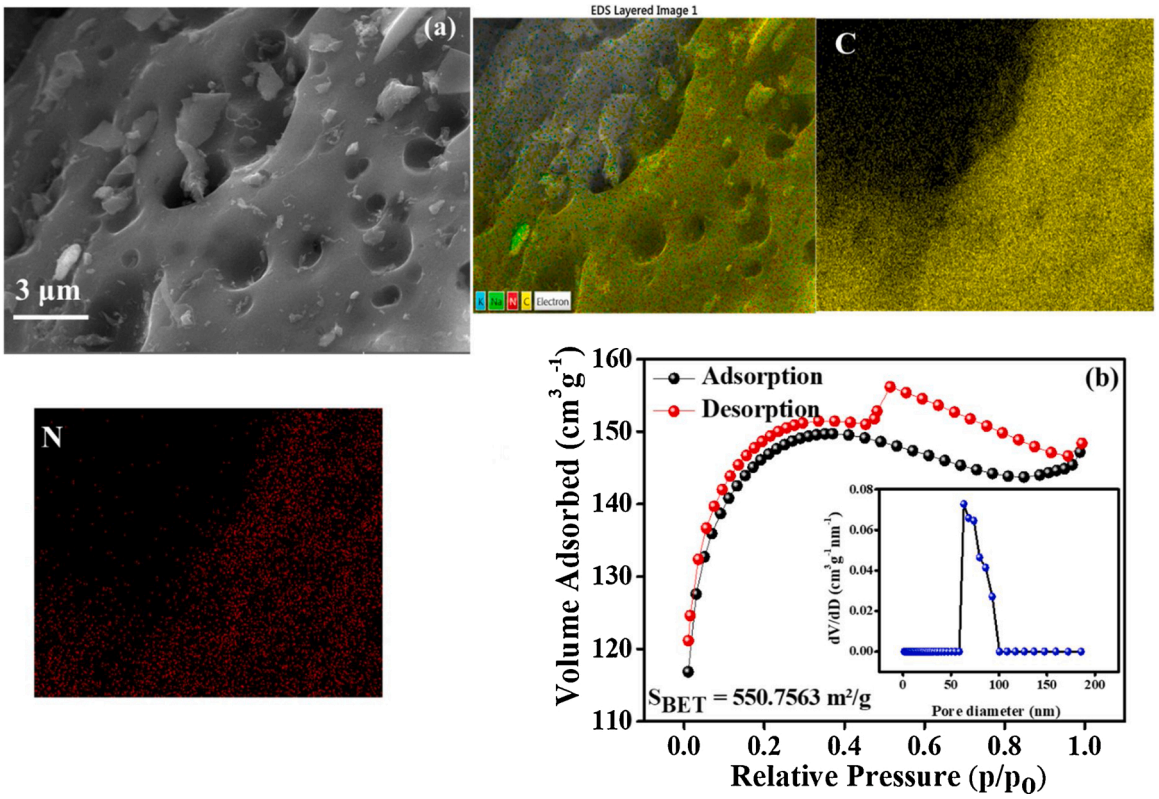

Fig. 2. (a) SEM image, and EDS analysis of the CLC (elemental mapping, yellow: carbon, and red: nitrogen), and (b) nitrogen adsorption-desorption isotherms, and the corresponding pore size distribution (inset) for the CLC (For interpretation of the references to colour in this figure legend, the reader is referred to the web version of this article).

created a porous structure throughout the carbon. The EDS investigation conforms to the nitrogen present in the carbon. The as-prepared CLC with nanoholes feature was inspected by Brunauer-Emmett-Teller (BET) characterization via adsorption and desorption of nitrogen. Fig. 2(b) shows the pore size distribution performed in the Barrett-Joyner-Halenda. The adsorption isotherm revealed a typical H3-type hysteresis loop, and the isotherm seems between the partial pressures (p/p_o) of 0.5–1.0 presence of the capillary concentration in the porous networks. The as-prepared CLC with nanoholes has the main pore distribution between 40–110 nm with an average pore size of 90.3 nm, and the surface area is approximately 550.75 $m^2 g^{-1}$. These porous networks not only increases the specific surface area but also increases the ionic conductivity by increasing the contact area between electrolyte and electrode; and enhancing the electrochemical performance of the Li-S batteries.

Fig. 3 illustrates the microstructure and morphology of the as-prepared CLC and CLC/S analyzed by FE-TEM. Fig. 3(a) illustrates the holes in the CLC observed by high magnification TEM. Fig. 3(b) shows the TEM image in high magnification, the number of nanoholes presented in the as-prepared carbon material from egg white indicated the formation of many nanoholes. As a result, the CLC has a high specific surface area and porosity. Fig. 3(c) shows only a few holes present in the CLC/S, indicating the sulfur successfully injected into the nanoholes of the CLC.

Fig. 4 illustrates the thermal stabilities of CLC/S composite by thermogravimetric analyses (TGA). The CLC/S sample was tested from room temperature to 500 °C in an N_2 atmosphere. The curve indicates the evaporation of the sulfur. The content of sulfur in the sample was evaluated to be approximately 78 wt%.

Fig. 5 indicates the electrochemical properties of the UC/S and CLC/

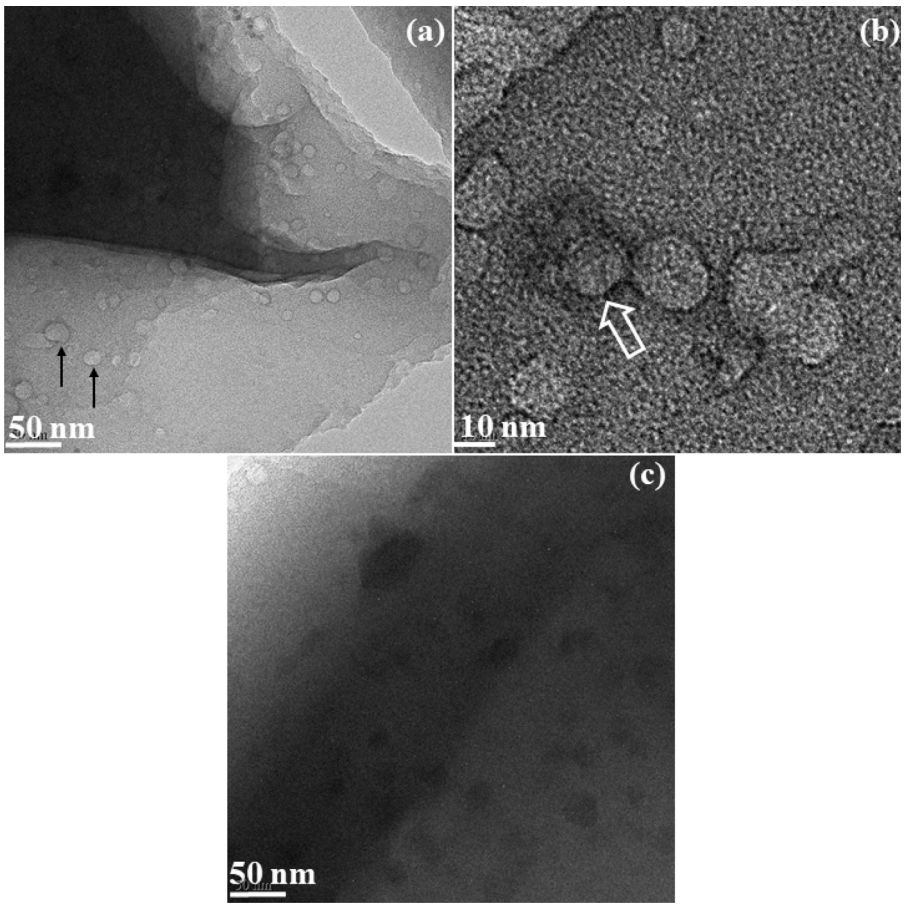

Fig. 3. TEM images of (a&b) low and high magnification of CLC, and (c) CLC/S composite.

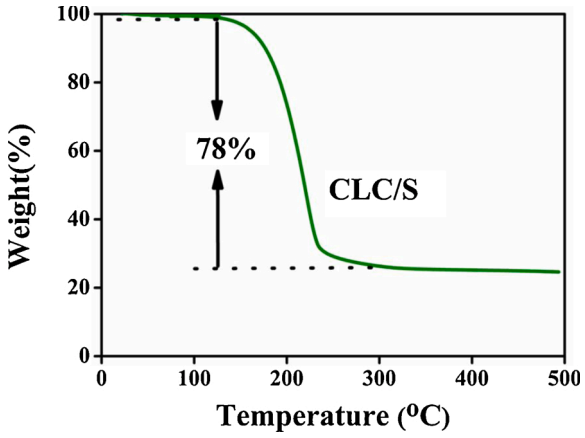

Fig. 4. Thermogravimetric analyses of CLC/S composite.

S performed by employing coin half cells. Fig. 5(a) shows the results of cyclic voltammetry (CV) carried out in the voltage range of 1.7–2.8 V at a scan rate of 0.1 mV s^{-1}. In the cathodic scan of the CLC/S electrode, the formation of long-chain lithium polysulfides occurs at 2.18 V. The long-chain polysulfides are converted to short-chain insoluble lithium sulfides at 1.99 V. In the anodic scan, short-chain polysulfides converted to sulfur at 2.55 V. UC/S shows two cathodic peaks at 2.2 and 2.0 V. The CLC/S electrode exhibits the smaller potential gaps between the redox peaks (2.18−1.99 V) and a higher intensity of the current (0.5 A) which signifies its faster reaction kinetics compared with UC/S. This favorable feature can be ascribed to the highly porous structure, which helps accelerate electron/ion transportation [23]. Fig. 5(b and C) shows the charge-discharge profiles of the CLC/S and UC/S electrodes at different C-rates. When comparing both electrodes, the CLC/S electrode showed the reduction of the discharge voltage platform and the increase of electrochemical polarization along with the intensifications of C-rates. However, at 2.18 V, the CLC/S electrode was showed a high capacity value of up to 600 mA h/g (the theoretical capacity is approximately 420 mA h/g). This high capacity is attributed to the nanoholes present in the carbon, complex side reactions, and the higher surface activity caused by the high specific surface area of the CLC [21,24–26]. Still, CLC/S achieved a relatively high discharge capacity of 425 mA h/g at a C-rate of 2 C. The CLC/S shows the high initial capacity ascribed to the good ionic transportation from the nanoholes and the desirable Li^+ ion conductivity from the high specific surface area. Moreover, the high pore volume can increase sulfur loading and equal distribution, thus improving the utilization of sulfur during cycling [27].

Fig. 5(d) shows the 50 cycles of the CLC/S and UC/S cathodes at 0.1 C-rates. The UC/S shows the lowest cycling capacities from the initial cycle (1397 mA h/g) to 50 cycles (74 mA h/g). The case of CLC/S shows a better cycling performance than the UC/S from initial cycling (1420 mA h/g) to the 50th cycle (400 mA h/g) with high coulombic efficiency. These results demonstrate the nanoholes of the CLC which gives strong interactions for polysulfide due to the capillary force [28,29]. Fig. 5(e) explains the rate capability of the CLC/S and UC/S cathodes. The CLC/S displays discharge capacities of 1420, 917, 686, 425, 464 mA h/g while the UC/S shows relatively low capacities of 1397, 274, 107, 110, 240 mA h/g at the C-rates of 0.1, 0.5, 1, 2 and 0.1 C, respectively. This implies that the CLC/S cathodes possess considerable stability and better reversibility than the UC/S. This is mainly ascribed to its cheese-like structure, which gives a high specific surface area for close

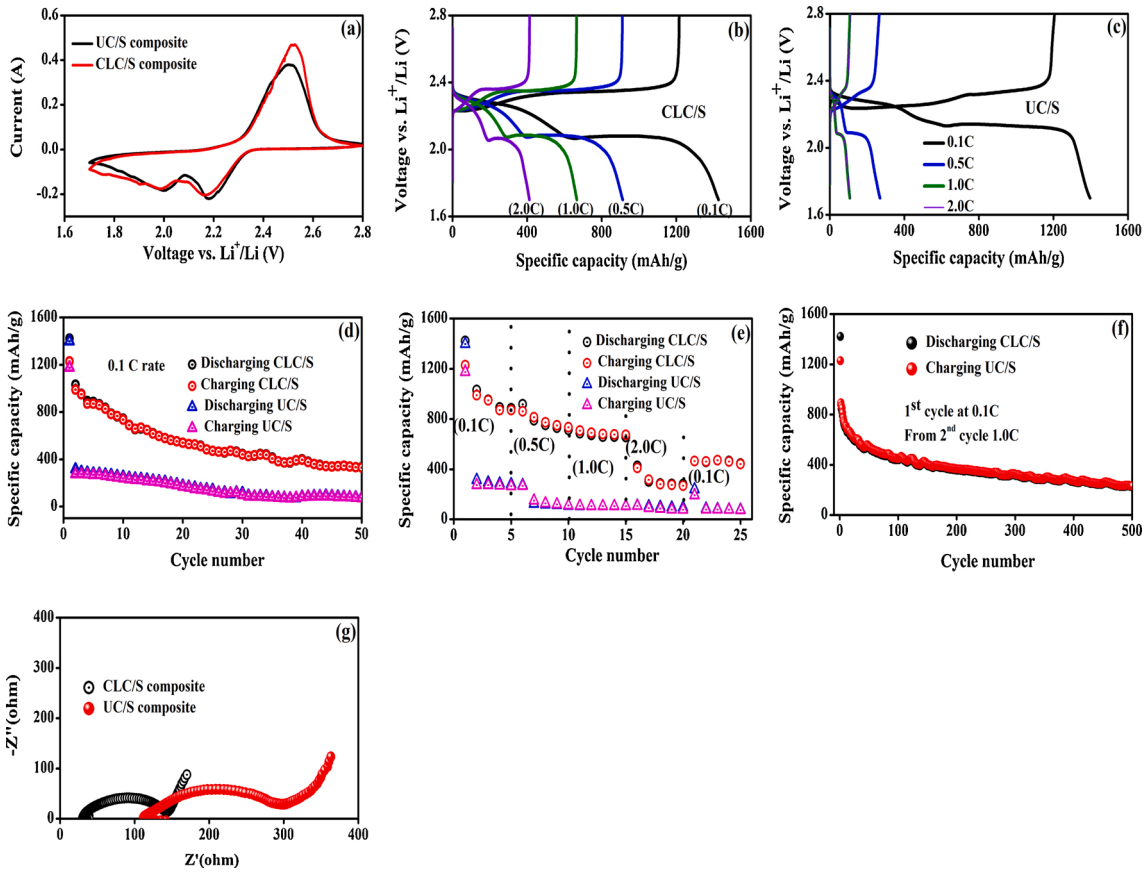

Fig. 5. (a) CV curves of UC/S, and CLC/S electrodes at a scanning rate of 0.1 mV/s, (b, and c) charge, and discharge voltage profiles of CLC/S, and UC/S electrode at different C-rates, (d) cyclic performance of CLC/S and UC/S electrodes at 0.1 C, (e) rate performance of CLC/S, and UC/S electrodes at different C-rates, (f) cyclic performance of CLC/S electrode at 1.0 C, and (g) **EIS** of CLC/S and UC/S electrodes.

interactions between the cheese-like conductive carbon and sulfur. The carbon has a high pore volume for the penetration of electrolytes and the volume expansion during cycling performances. However, after returning to the 0.1C-rate, the CLC/S electrode shows the capacity loss, which can also be attributed to the lithium dendrite caused by soft short [29]. Fig. 5(f) illustrates the cycling performance of the CLC/S cathode first cycle investigated at 0.1 C and from the second cycle at 1 C-rate. The CLC/S shows a 275 mA h/g discharge capacity for the 500th cycle with 98 % coulombic efficiency. These results demonstrate the good structural properties of the CLC host material for the inhibition of the shuttle effect and the improvement of sulfur reaction reversibility through a combination of chemical and physical sulfur confinements. Fig. 5(g) shows the Nyquist plots of the UC/S and CLC/S electrodes. The semi-circle in the figure results in the resistance of the charge transfer (R_{ct}) [30]. The R_{ct} for the UC/S and CLC/S cell is 300 Ω and 150 Ω, respectively. The EIS curve indicates that the CLC/S electrode has good conductivity and high catalytic activity than the UC/S electrode. The lower value of R_{ct} of CLC/S indicates the faster ion/electron transportation and sulfur reaction kinetics at the electrode interfaces.

4. Conclusions

In summary, sulfur has been successfully inserted in CLC with nanoholes fabricated from a boiled white egg via a simple annealing procedure. Here, a cheese-like structure can suppress the polysulfide and increases the usage of sulfur. During the charge-discharge process, the CLC in the sulfur composite increases the conductivity and ion transport capability. The prepared CLC buffered the volume expansion during cycling, which resulted in enhanced excellent cycling performance and stability. The specific capacity was 275 mA h/g after 500 cycles at 1 C-rate. CLC with nanoholes and doped sulfur is the most promising cathode material for energy storage applications.

Authorship statement

B.S. Reddy: Investigation, Methodology, and writing original draft. **M. Premasudha:** Investigation. **Kwang-Moon oh:** Methodology. **N.S. Reddy:** English correction and review. **Jou-Hyeon Ahn:** Conceptualization, Supervision, Writing - review & editing. **Kwon-Koo Cho:** Conceptualization, Supervision, Writing - review & editing.

Declaration of Competing Interest

The authors declare that they have no known competing financial interests or personal relationships that could have appeared to influence the work reported in this paper.

Acknowledgments

This research was supported by the project (NRF-2019R1A2C1086610) through the National Research Foundation of Korea (NRF) by the Ministry of Science, ICT & Future Planning (MSIP) and the National Research Foundation of Korea (NRF) funded by the Ministry of Education (NRF-2020R1A6A1A03038697).

References

[1] J. Chen, L. Xu, W. Li, X. Gou, Adv. Mater. 17 (2005) 582–586.
[2] S. Liu, X. Xia, S. Deng, D. Xie, Z. Yao, L. Zhang, S. Zhang, X. Wang, J. Tu, Adv. Mater. 31 (2019) 1806470.

[3] Y. Zhong, X. Xia, S. Deng, J. Zhan, R. Fang, Y. Xia, X. Wang, Q. Zhang, J. Tu, Adv. Energy Mater. 8 (2018), 1701110.
[4] J. Wen, Y. Yu, C. Chen, Mater. Express 2 (2012) 197–212.
[5] T.Z. Zhuang, J.Q. Huang, H.J. Peng, L.Y. He, X.B. Cheng, C.M. Chen, Q. Zhang, Small 12 (2016) 381–389.
[6] M. Wild, L. O'neill, T. Zhang, R. Purkayastha, G. Minton, M. Marinescu, G. Offer, Energy Environ. Sci. 8 (2015) 3477–3494.
[7] J. Zhang, C.P. Yang, Y.X. Yin, L.J. Wan, Y.G. Guo, Adv. Mater. 28 (2016) 9539–9544.
[8] H.J. Peng, J.Q. Huang, X.B. Cheng, Q. Zhang, Adv. Energy Mater. 7 (2017), 1700260.
[9] S.H. Chung, A. Manthiram, Adv. Mater. 26 (2014) 7352–7357.
[10] P. Barai, A. Mistry, P.P. Mukherjee, Extreme Mech. Lett. 9 (2016) 359–370.
[11] G. Ren, S. Li, Z.-X. Fan, J. Warzywoda, Z. Fan, J. Mater. Chem. A 4 (2016) 16507–16515.
[12] J. Qu, S. Lv, X. Peng, S. Tian, J. Wang, F. Gao, J. Alloys. Compd. 671 (2016) 17–23.
[13] W. Li, Z. Liang, Z. Lu, H. Yao, Z.W. Seh, K. Yan, G. Zheng, Y. Cui, Adv. Energy Mater. 5 (2015), 1500211.
[14] Y. Yan, Y. Wei, Q. Li, M. Shi, C. Zhao, L. Chen, C. Fan, R. Yang, Y. Xu, J. Mater. Sci. Mater. Electron. 29 (2018) 11325–11335.
[15] X. Gu, Y. Wang, C. Lai, J. Qiu, S. Li, Y. Hou, W. Martens, N. Mahmood, S. Zhang, Nano Res. 8 (2015) 129–139.
[16] Z. Sun, S. Wang, L. Yan, M. Xiao, D. Han, Y. Meng, J. Power Sources 324 (2016) 547–555.
[17] H. Ding, J. Zhou, A.M. Rao, B. Lu, Sci. Rev. (2020).
[18] Y. Feng, S. Chen, J. Wang, B. Lu, J. Energy Chem. 43 (2020) 129–138.
[19] Q. Zhang, X. Cheng, C. Wang, A.M. Rao, B. Lu, Energy Environ. Sci. (2020).
[20] H. Wu, L. Xia, J. Ren, Q. Zheng, C. Xu, D. Lin, J. Mater. Chem. A 5 (2017) 20458–20472.
[21] X. Yuan, L. Wu, X. He, K. Zeinu, L. Huang, X. Zhu, H. Hou, B. Liu, J. Hu, J. Yang, Chem. Eng. J. 320 (2017) 178–188.
[22] L. Luo, A. Manthiram, ACS Energy Lett. 2 (2017) 2205–2211.
[23] S. Yan, J. Wu, Y. Dai, Z. Pan, W. Sheng, J. Xu, K. Song, Colloids Surf. A Physicochem. Eng. Asp. 591 (2020), 124513.
[24] J.M. Chabu, K. Zeng, G. Jin, M. Zhang, Y. Li, Y.-N. Liu, Mater. Chem. Phys. 229 (2019) 226–231.
[25] S. Wang, H. Wang, R. Zhang, L. Zhao, X. Wu, H. Xie, J. Zhang, H. Sun, J. Alloys. Compd. 746 (2018) 567–575.
[26] Y. Zhu, G. Xu, X. Zhang, S. Wang, C. Li, G. Wang, J. Alloys. Compd. 695 (2017) 2246–2252.
[27] Q. Xiao, G. Li, M. Li, R. Liu, H. Li, P. Ren, Y. Dong, M. Feng, Z. Chen, J. Energy Chem. 44 (2020) 61–67.
[28] C. Yan, X.-B. Cheng, C.-Z. Zhao, J.-Q. Huang, S.-T. Yang, Q. Zhang, J. Power Sources 327 (2016) 212–220.
[29] Y. Hu, W. Chen, T. Lei, Y. Jiao, H. Wang, X. Wang, G. Rao, X. Wang, B. Chen, J. Xiong, Nano Energy 68 (2020), 104373.
[30] L. Ma, W. Zhang, L. Wang, Y. Hu, G. Zhu, Y. Wang, R. Chen, T. Chen, Z. Tie, J. Liu, Z. Jin, ACS Nano 12 (2018) 4868–4876.